Astronomy & Astrophysics manuscript no. output
July 4, 2024

The Rotational Velocity of Stars with Exoplanets

Carolina Malheiro

Institute of Astrophysics and Space Sciences (IA) - Centro de Astrofísica da Universidade do Porto (CAUP)

ABSTRACT

The characterization of stars is a crucial step for the study of many Astrophysics topics, in particular for the characterization of planetary systems. The rotational velocity is a specific characteristic that is important to understand the age of these systems and their birth environment. We aim to complement the Stars With ExoplanETs Catalogue (SWEET-Cat) with relevant information about the rotational velocity of stars that host planets, for which there is good spectroscopic data. To this goal, we derive the *vsini* of these stars, through the analysis of the width of spectral lines, using a program implemented in Python which works with other spectroscopic tools such as MOOG. In this project, we tested the code to understand its reliability and possible dependences on stellar parameters such as temperature, metallicity, surface gravity and macroturbulence velocity. Taking into account the results, we concluded that this is, generally, a good method to derive *vsini*, with no specific correlation to the stellar features mentioned. However, for stars with lower velocities there are some adjustments needed, which could be found in the future.

1. Introduction

In the last decades, there has been a growth in the study of exoplanetary systems, with the detection of several stars that host planets. So, with this increase, it is important to understand how these systems initially begin and evolve. One relevant characteristic that can tell us more about these environments is the rotational velocity of the host star. (Addison et al. 2020), (Santos et al. 2013)

By analysing spectral line profiles we can obtain information about the physical structure of the star. In particular, we can determine the stellar radial velocity and velocity fields, such as macro and microturbulence.

Taking into account that stars rotate around an axis, this brings some effects to its observed spectrum. These are very small in the continuum, but noticeable in the spectral lines, due to the Doppler shift of the light coming from different parts of the stellar disk. As a result, the part of the limb that is approaching is blue shifted and the one receding is red shifted, as we can see in figure 1.

Furthermore, it must be noted that the rotation axis is arbitrary and, in fact, the Doppler effect will depend on the angle between the axis and the line of sight of the observer. As such, the real velocity measured through the spectral lines is *vsini*, the component of the velocity along the line of sight, *i* being the angle refered before (figure 2). In cases that *i* is 90º, we expect to be seeing the real velocity just with shifts, for smaller angles the velocity will be reduced comparatively to the real one, and reaching 0º no rotation will be noted.

There are two main methods to determine the *vsini* of a star through its spectrum: Fourier analysis or profile fitting. In this project, we focus on the second procedure, comparing the spectra of stars to synthetic rotational profiles with well defined parameters. (Catanzaro 2014), (Gray 2005)

This technic was implemented in a program written in python which, through MOOG, synthesises line profiles with known characteristics of the star, and then compares the real one with each of these to determine which one has the closest velocity. Figure 3 is a visual represention of these computations, with several lines being compared to the original one.

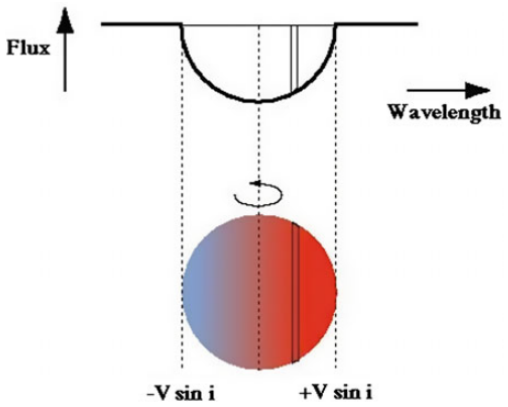

Fig. 1. Schematic view of the Doppler broadening of a spectral line due to rotation. (Catanzaro 2014)

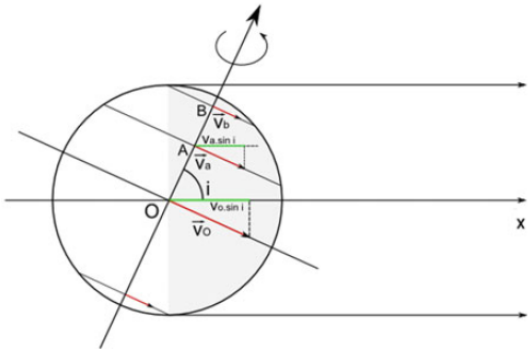

Fig. 2. Schematic view of the decomposition of the real velocity in components along the line of sight (x). *i* is the angle between the rotational axis and x. (Catanzaro 2014)

2. Testing *vsini_code*

Throughout this project, there were two main parts. First, we tested previous codes to understand if they worked in the best way or if there was a need to make some modifications. The pro-

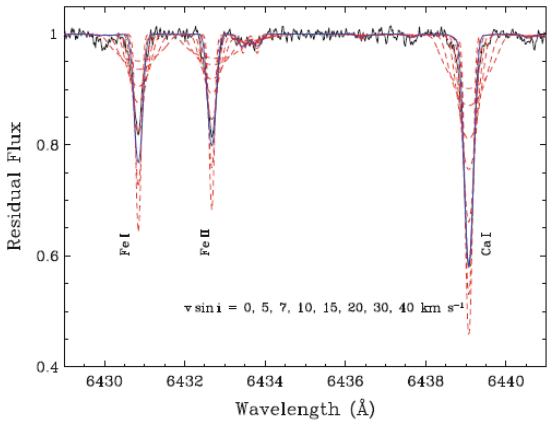

Fig. 3. Part of an observed spectrum with synthetic spectra overimposed. Each artificial profile has a different *vsini*, being the best value 7 km/s. (Catanzaro 2014)

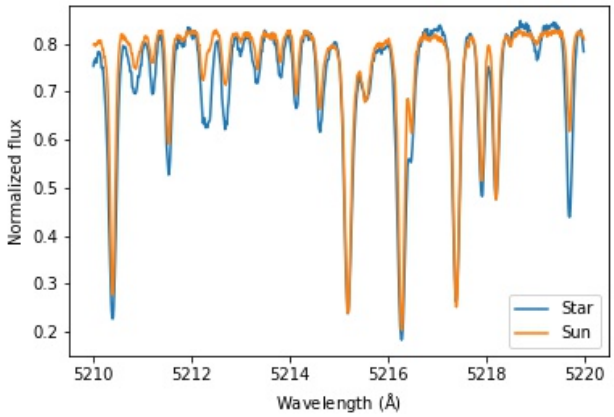

Fig. 4. Corrected spectrum of star TYC 3667-1280-1 compared to the Sun.

Star	vsini (extr)	vsini
38Vir	28.767	28.767
CoRoT-11	42.829	42.829
HATS-58A	4.596	4.596,
XO-7	5.933	5.933
HD12484	11.182	11.182
Kepler-435	7.642	7.642
Kepler-539	8.862	8.862
Kepler-74	4.999	4.999

Table 1. Extrapolation.

grams tested are the ones used previously by another colleague, with some small alterations, based on the results and problems encountered throughout.

To derive the value of the rotational velocity, we used a program written in python (*vsini_code* that can be accessed in https://github.com/cmal95/PEEC2024) which analyses the spectrum of a star and, considering some parameters (effective temperature of the star and respective uncertain (Teff and eTeff), surface gravity (logg), metallicity and respective uncertain ([Fe/H] and e[Fe/H]), turbulence velocity (vtur) and intrumental broadening (inst_broad)), calculates the velocity. In a simple manner, this algorithm reads the spectrum of a certain star, synthetizes several spectra with different velocities through MOOG, and, finally, compares them to the original spectrum to see which value must be the closest to the real one.

Another value needed was the macroturbulence, which was calculated in the program itself using equation 1 for the temperature between 5000 K and 6500 K, and assuming 2.2km/s and 5.5km/s, respectively, for values below or above these limits. (Doyle 2014)

$$v_{mac} = 3.21 + 2.33x10^{-3}(T_{eff} - 5777) + 2x10^{-6}(T_{eff} - 5777)^2 - 2(logg - 4.44) \quad (1)$$

However, an important step that was done for each spectrum was the correction of the radial velocity. To this end, we used a program (*correction_vr*) that compared the line profile we wanted to correct with a reference, in this case, a spectrum from the Sun, because of its optimal values. Using a cross-correlation function from *PyAstronomy*, we obtained the best value for the radial velocity and, then, recalculated and rewrote the spectrum for the corrected velocity, using equation 2, where λ is the real wavelength, λ_{obs} is the observed wavelength, RV is the radial velocity calculated through cross-correlation and c is the speed of light. As may be seen as an example in figure 4, the spectrum was aligned with the sepctrum of the Sun.

$$\lambda = \frac{\lambda_{obs}}{1 + RV/c} \quad (2)$$

Then, with the spectra corrected, it was possible to implement *vsini_code*. All the parameters needed as input for the function were obtained from the SWEET-Cat (SWEET-Cat), (Sousa et al. 2021). The instrumental broadening was calculated from equation 3, where $\Delta\lambda$ is the instrumental broadening, R is the spectograph's resolution and λ is the wavelength, which, in this case, was considered as the half value of the range of the spectra.

$$\Delta\lambda = \frac{\lambda}{R} \quad (3)$$

During the first atempts to obtain values, we came across an error, with data out of the interpolation range, that we managed to solve using extrapolation. To understand if this would bring some alteration to the results, we derived values without extrapolation for some stars that worked both ways. In table 1 and figure 5, it is possible to see that extrapolation was a good option, yielding exactly the same results, including the error.

After we started obtaining the solutions, another error was encountered, related to the calculation of the limb darkening coefficient. Originally, it was evaluated through an interpolation function which used a certain range of predetermined coefficients, depending on the effective temperature, the logarithm of acceleration of gravity and the metallicity, whose ranges were: T_{eff}:[3500,7000[, logg:[3.0,5.0[, FeH:[-0.5,0.5[. However, some of the stars had values out of the range of those already registered, so it was necessary to get them some other way. We used the Exoplanet Characterization Toolkit (ExoCTK), which had also been used before for the predetermined ones, and obtained specific coefficients for the stars that needed it.

With all these corrections, it was finally possible to make a full derivation of the rotational velocity.

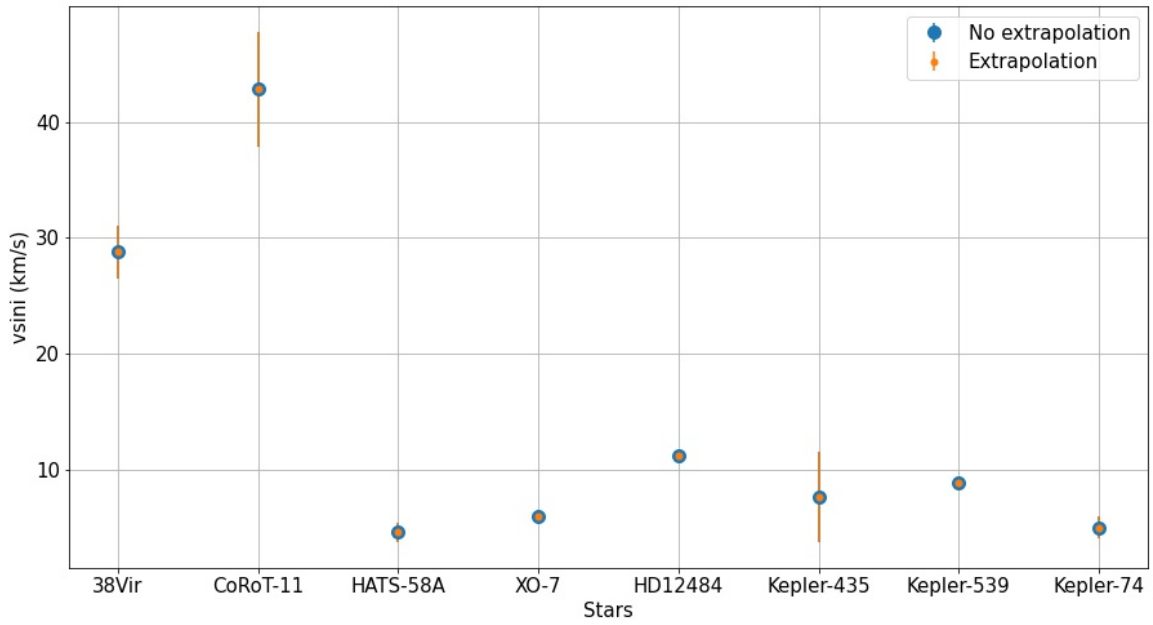

Fig. 5. Extrapolation.

3. Results and analysis

In the second part of the project, we evaluated the *vsini* for two distinct groups of stars. The first one had been used before, so it was possible to compare both with the literature results and previous versions of the programs. In the first one, the expected rotational velocities were more varied, with higher and smaller values. As for the second group, the literature values were generally lower, at most 5 km/s. All the results and star information used can be accessed in https://github.com/cmal95/PEEC2024.

In general, all the stars in the first group yielded good results, almost always within error of the reference values, which were obtained from NASA exoplanet archive (NASA Archive), however, the second set produced much more deviated results. In figure 6, it can be seen the superposition of the values and the respective error bars, noting the pronouncement refered before between the stars XO-7 and TYC 3667-1280-1. In figure 7, we can observe the difference between our results and the reference values, once again with a more visible deviation from $y = 0$ between the two stars mentioned above.

Taking into account these results we can infer that there's a bigger difficulty in deriving the rotational velocities for the cases in which it appears to be smaller, possibly because in these cases the superposition of all the sources of error are more blended and harder to differentiate.

To understand where this error may occur, it was made an analysis of how the results depended on certain stellar parameters, such as the temperature, the metallicity, the logarithm of the gravitational acceleration and the velocity of macroturbulence. Table 2 shows the values of the linear regressions for these parameters, regarding the rotational velocity from MOOG, whereas Table 3 presents the parameters of the linear regressions for the difference between the results we obtain using MOOG and the values with which we compared in the literature.

In figure 8, we can observe the dependence of *vsini* on the effective temperature, and, as expected, there's a slight growth

Parameter	b(km/s)	a	R^2
Teff	-10.613	0.003	0.143
vmac	-0.197	1.587	0.166
logg	1.166	1.162	0.025
feh	5.920	0.667	0.0008

Table 2. Linear regressions for the absolute velocities derived using MOOG. The parameters b, a and R^2 are, respectively, the intercept, the slope and the coefficient of determination.

Parameter	b(km/s)	a	R^2
Teff	3.034	-0.0005	0.031
vmac	0.993	-0.166	0.015
logg	3.473	-0.754	0.085
feh	0.444	-0.961	0.013

Table 3. Linear regressions for the difference between MOOG results and literature. The parameters b, a and R^2 are, respectively, the intercept, the slope and the coefficient of determination.

on the velocity as the temperature also increases, however it is not a totally linear dependence. Regarding the differences, we can see that they are not directly related to the temperature of the stars, with a slope and R^2 very close to 0.

Another parameter which we thought to inspect was the macroturbulence velocity. The linear regressions can be seen in figure 9. As for the temperature, there appears to be a rough growth of the velocity accompanying the increase in macroturbulence velocity, which is an expected result, taking into account that both are dependent on the temperature, nevertheless it is not possible to establish a complete relation. When we look at the results for the differences in *vsini*, it is possible to conclude that these deviations are completely independent of the *vmac*.

Similar analysis can be made for two other parameters, metallicity and the logarithm of acceleration of gravity. Figures

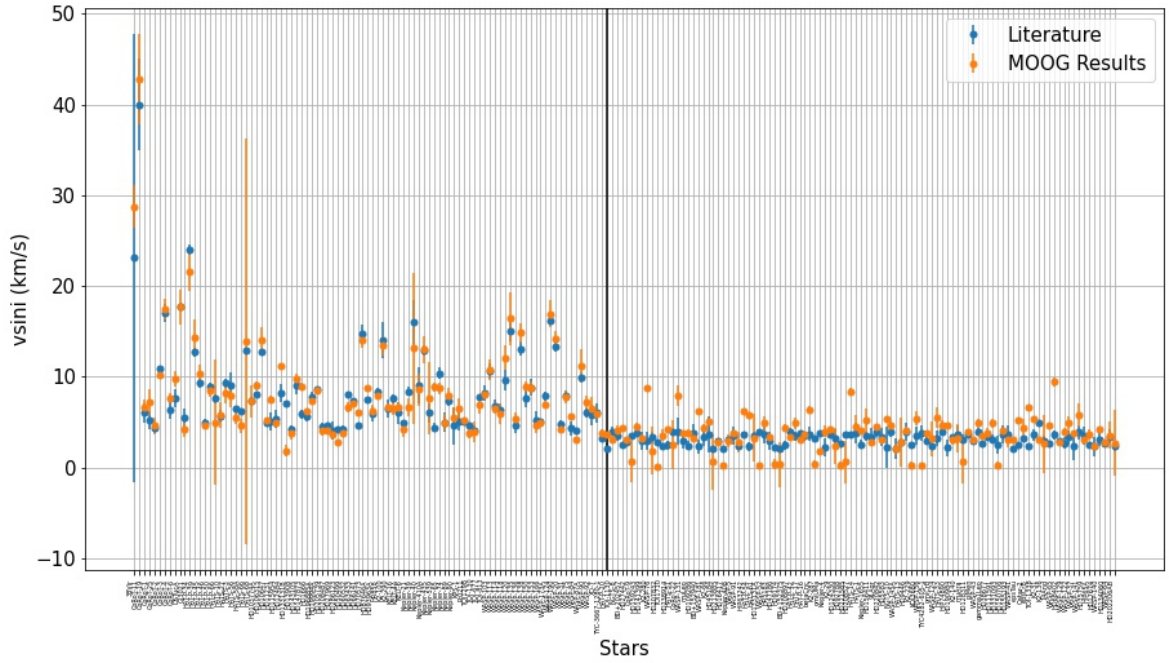

Fig. 6. Comparison between MOOG results and literature values for all the stars.

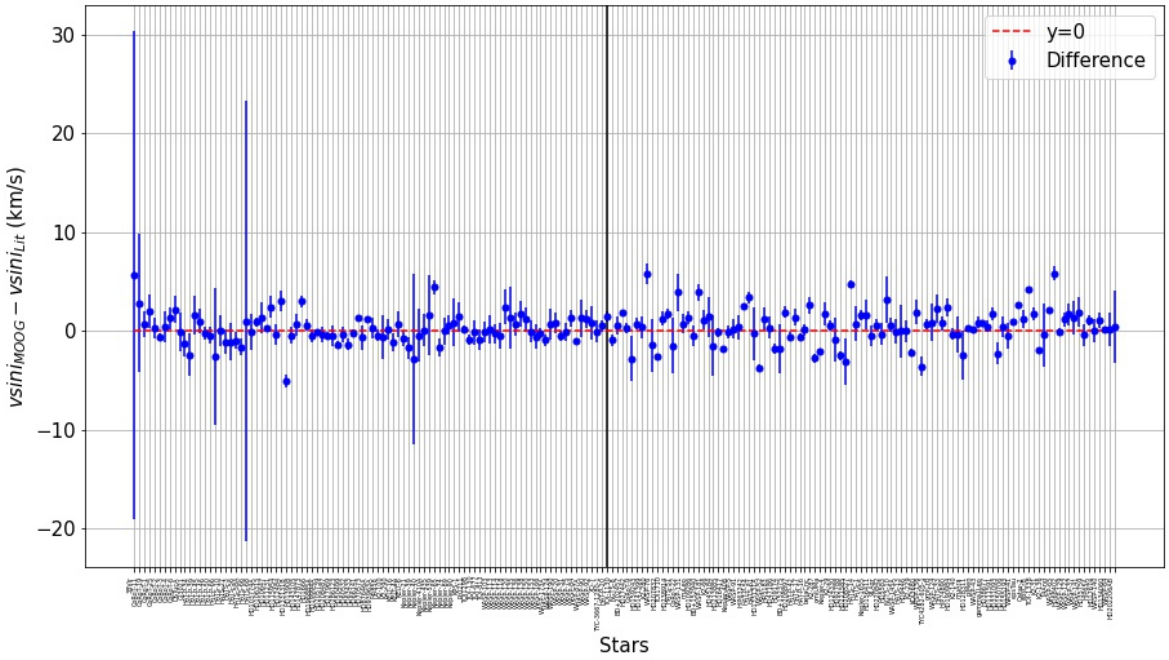

Fig. 7. Difference between the MOOG results and the literature values.

10 and 11 demonstrate the dependences for these two stellar characteristics. For both of them, considering also the linear regresion parameters, we can deduce that there is no linear relation to the velocities that were calculated.

4. Other observations

The discussion done before regarded values that were considered good estimations, even if their deviation from literature was bigger than the estimated errors. However, there was a group of values which was not included in the previous analysis because they were too deviated and, as such, were considered as outliers. These results and the respective stellar characteristis can be ob-

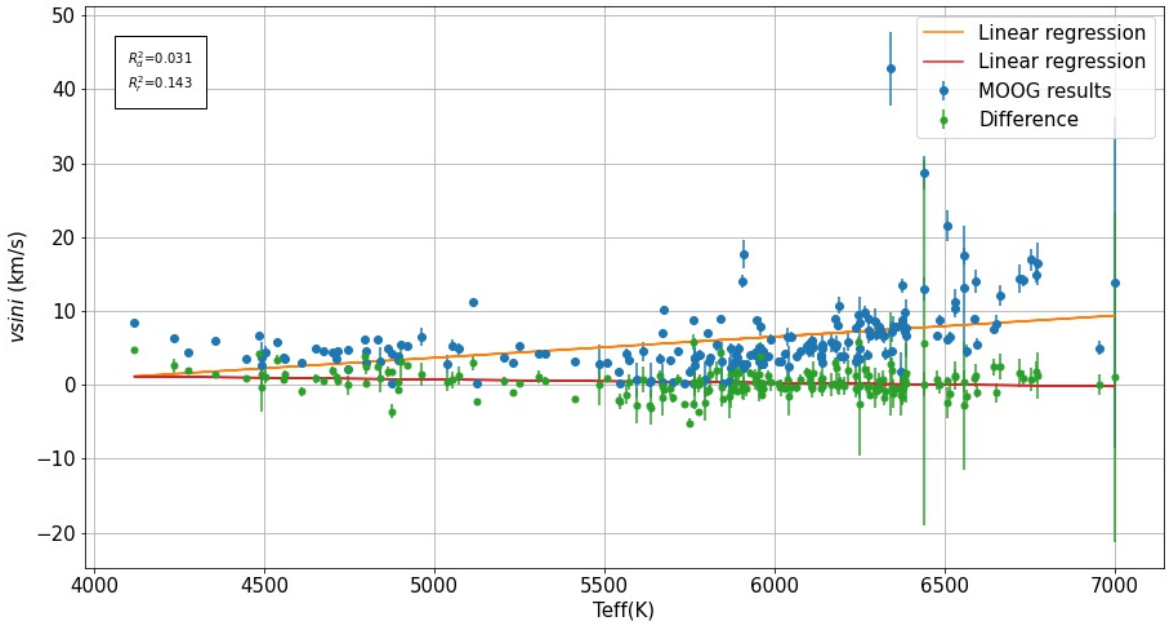

Fig. 8. Dependence of the velocities on the temperature. In blue are the MOOG results, with the respective linear regression in orange(R^2 = 0.143). In green are the differences bewtween MOOG and literature, with its linear regression in red (R^2 = 0.031).

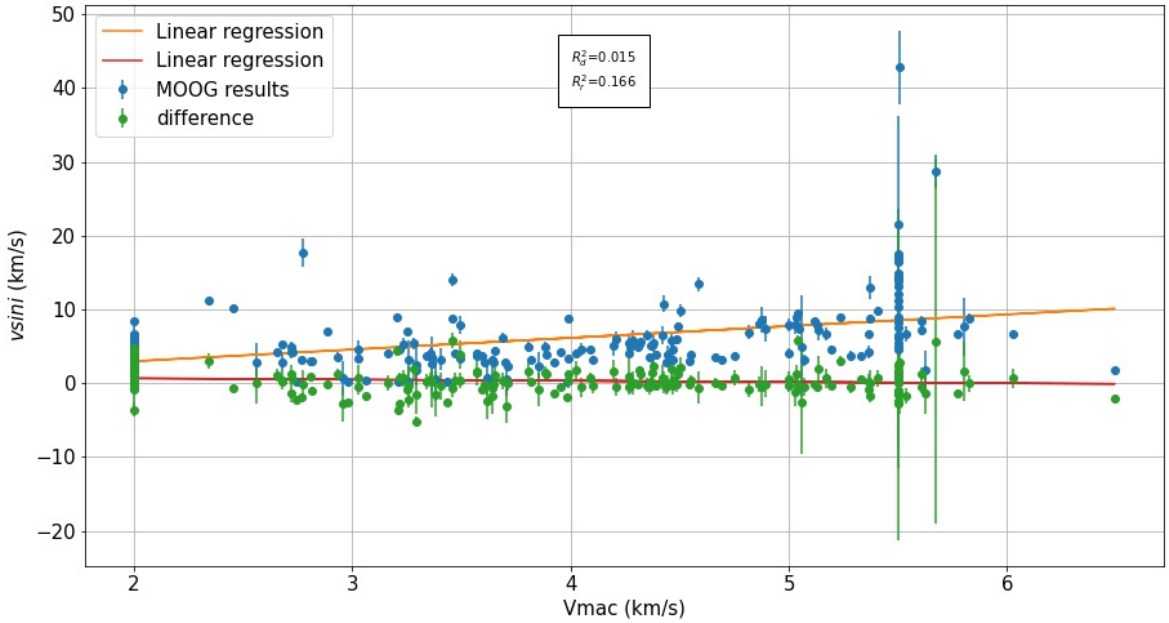

Fig. 9. Dependence of the velocities on the macrotubulence velocity. In blue are the MOOG results, with the respective linear regression in orange(R^2 = 0.166). In green are the differences bewtween MOOG and literature, with its linear regression in red (R^2 = 0.015).

served in Table A.1. The values that were excluded range from 0.1 km/s, the lower limit, 10.537 km/s and 29.879 km/s, which were considered too big for those two stars, and 50.0 km/s, the higher limit.

The main problem observed was that, for many stars, the value of the velocity obtained was in the lower limit, mostly with an error of 0.0. It is possible to understand that these values can't be right and there must be a source of error in the calculation or in the initial parameters. In the period of this project it wasn't

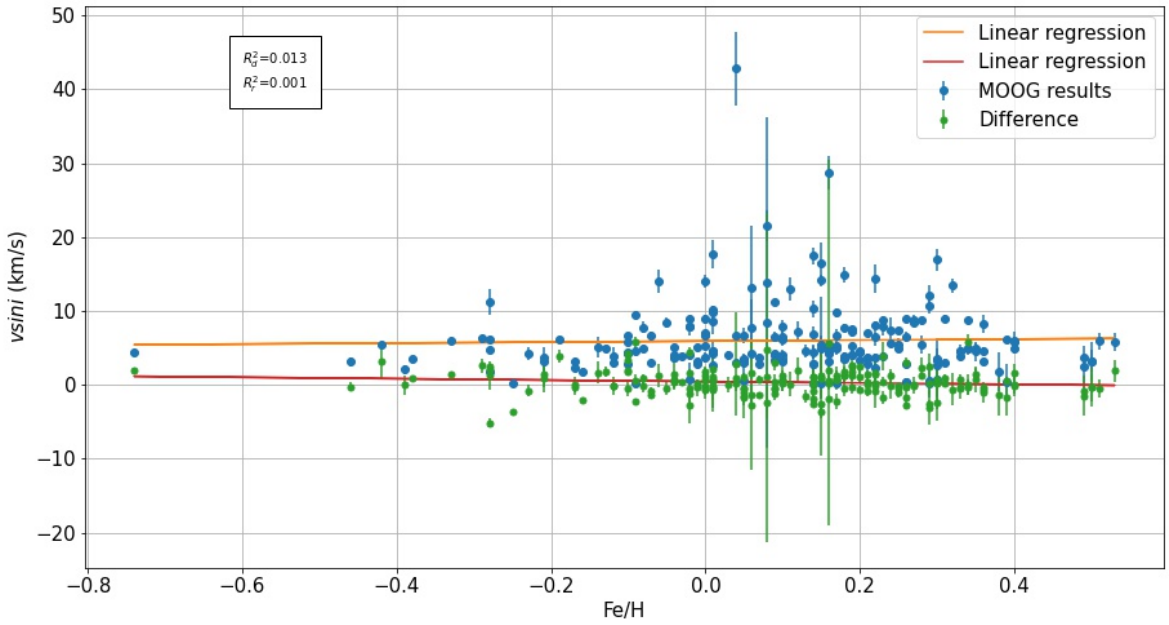

Fig. 10. Dependence of the velocities on the metallicity. In blue are the MOOG results, with the respective linear regression in orange(R^2 = 0.001). In green are the differences bewtween MOOG and literature, with its linear regression in red (R^2 = 0.013).

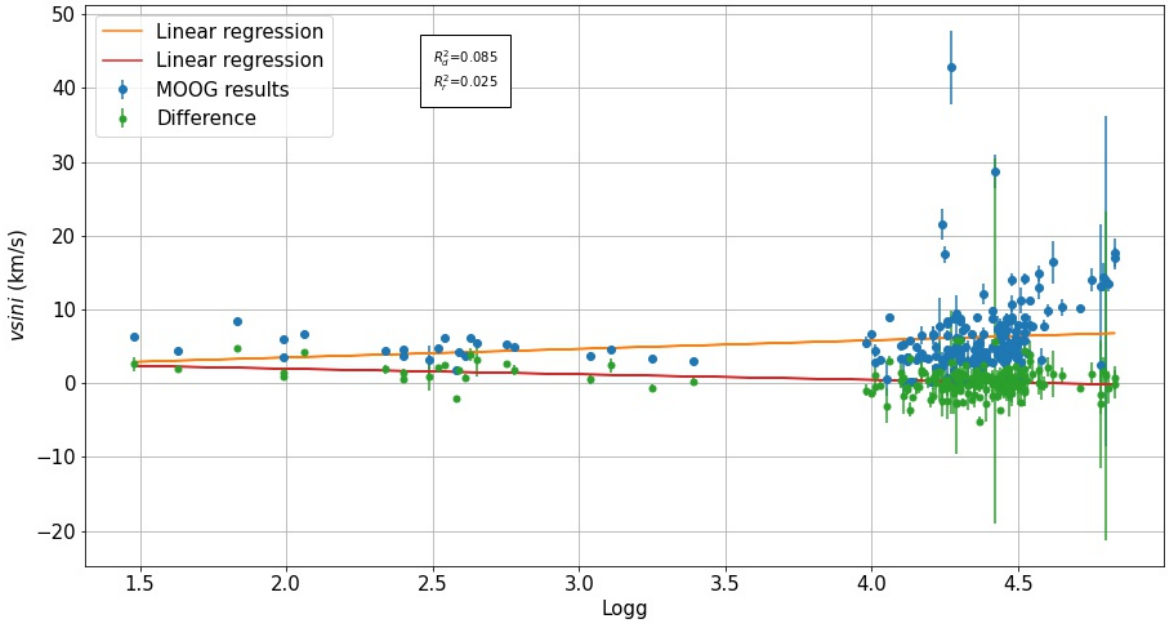

Fig. 11. Dependence of the velocities on the logarithm of acceleration of gravity. In blue are the MOOG results, with the respective linear regression in orange(R^2 = 0.025). In green are the differences bewtween MOOG and literature, with its linear regression in red (R^2 = 0.085).

possible to conclude where this issue came from. We thought of the macroturbulence velocity, since it is somewhat close related to *vsini*, it may be overestimated in our code, robbing some value from the rotation velocity. Otherwise, the initial parameters may not be completely right, bringing complications to the estimation.

Even so, it must be remarked that it is mostly sytematic for low velocities, this is specially important, if we remember that the worst of the acceptable results were also for slow stars. Adi-

tionally, it should be mentioned that a parameter of convergence in the code, *status*, almost always gave the value 4. This was not explored, yet it may shine a light on the solution for this problem in the future.

5. Conclusion

In this project, it was possible to understand the importance of characterizing stars to find exoplanets, in specific its rotational velocity. This property helps determine the age and origin of the planetary system, allowing for better conclusions. As such, we tested a python program that uses MOOG as a tool to determine the *vsini* of stars.

The results obtained grant us a great degree of confidence in this tool, with mostly values within error of other calculations done with other methods, registered in the literature we compared with. Furthermore, any slight discrepancies don't appear to have any close relation to other stellar traits, such as temperature, metallicity, acceleration of gravity and macroturbulence velocity.

Notwithstanding, it must be used with caution for slower stars, for which we found some errors and problems in the derivation. Not being possible to find an origin for these errors, it is expected and hoped that in the future, new conclusions and corrections may help.

References

[Addison et al. 2020] Addison, B. C., Wright, D. J., Nicholson, B. A., Cale, B., Mocnik, T., Huber, D., Plavchan, P., Wittenmyer, R. A., Vanderburg, A., Chaplin, W. J., Chontos, A., Clark, J. T., Eastman, J. D., Ziegler, C., Brahm, R., Carter, B. D., Clerte, M., Espinoza, N., Horner, J., … Themeßl, N. (2020). TOI-257B (HD 19916b): A warm sub-saturn orbiting an evolved F-type star. Monthly Notices of the Royal Astronomical Society, 502(3), 3704–3722.

[SWEET-Cat] SWEET-Cat: A catalog of stellar parameters for stars with planets. https://sweetcat.iastro.pt/

[Catanzaro 2014] Catanzaro, G. (2014). Spectral lines analysis: Rotational velocity and Velocity Fields. Determination of Atmospheric Parameters of B-, A-, F- and G-Type Stars, 121–130.

[Doyle 2014] Doyle, A. P., Davies, G. R., Smalley, B., Chaplin, W. J., & Elsworth, Y. (2014). Determining stellar macroturbulence using asteroseismic rotational velocities from Kepler. Monthly Notices of the Royal Astronomical Society, 444(4), 3592–3602.

[Gray 2005] Gray, D. F. (2005). The observation and analysis of Stellar Photospheres. Cambridge University Press.

[ExoCTK] Limb darkening calculator. ExoPlanet Characterization Tool Kit. (n.d.). https://exoctk.stsci.edu/limb_darkening

[NASA Archive] NASA exoplanet archive. NASA Exoplanet Archive. (n.d.). https://exoplanetarchive.ipac.caltech.edu/

[Santos et al. 2013] Santos, N. C., Sousa, S. G., Mortier, A., Neves, V., Adibekyan, V., Tsantaki, M., Delgado Mena, E., Bonfils, X., Israelian, G., Mayor, M., & Udry, S. (2013). Sweet-Cat: A catalogue of parameters for stars with exoplanets. Astronomy & Astrophysics, 556.

[Sousa et al. 2021] Sousa, S. G., Adibekyan, V., Delgado-Mena, E., Santos, N. C., Rojas-Ayala, B., Soares, B. M., Legoinha, H., Ulmer-Moll, S., Camacho, J. D., Barros, S. C., Demangeon, O. D., Hoyer, S., Israelian, G., Mortier, A., Tsantaki, M., & Monteiro, M. A. (2021). Sweet-Cat 2.0: The cat just got sweeter. Astronomy & Astrophysics, 656.

Appendix A: Parameters of stars and results

Star	Instr broad	T_{eff}	logg	Fe/H	vsini	v_{mac}	e_{vsini}
WASP-23	0.046	5077.0	4.36	0.06	10.5	2.719	0.443
GJ785	0.046	5041.0	4.34	-0.06	0.1	2.779	0.000
TOI-132	0.046	5368.0	4.33	0.26	0.1	2.812	0.000
HIP65407	0.072	5432.0	4.39	0.21	50.0	2.744	0.000
HD221416	0.046	5056.0	3.50	-0.13	0.1	4.450	0.000
HD11977	0.046	5018.0	2.85	-0.15	0.1	5.774	4.000
HD29021	0.072	5521.0	4.41	-0.27	0.1	2.805	0.000
HD164595	0.046	5714.0	4.36	-0.07	0.1	3.231	0.000
HD219666	0.046	5539.0	4.32	0.06	0.1	3.009	0.078
CoRoT-32	0.135	5859.0	4.59	0.06	0.1	3.115	0.000
HD44219	0.046	5772.0	4.21	0.06	0.1	3.658	0.000
HD108874	0.047	5597.0	4.33	0.21	0.1	3.075	0.000
WASP-59	0.135	4401.0	3.97	-0.02	0.1	2.000	0.000
NGTS-4	0.046	5122.0	4.27	-0.12	29.9	2.882	3.000
HD20794	0.046	5422.0	4.53	-0.42	0.1	2.455	0.000
Qatar-6	0.054	5930.0	4.46	-0.02	0.1	3.573	0.000
HIP109600	0.072	5503.0	4.32	-0.17	0.1	2.962	0.000
HD215152	0.046	4830.0	4.29	-0.09	0.0	2.000	0.000
BD+631405	0.072	5000.0	4.20	-0.09	0.1	2.000	0.174
TOI1296	0.047	5603.0	4.05	0.044	0.1	3.645	0.000
K2-27	0.046	5242.0	4.29	0.13	0.1	2.836	0.000
K2-285	0.047	5047.0	4.34	-0.05	0.1	2.775	0.000
CoRoT-28	0.135	5414.0	3.90	0.23	50.0	3.708	40.800
EPIC249893012	0.046	5567.0	4.03	0.16	0.1	3.629	0.181
24Sex	0.046	5014.0	3.22	-0.02	0.1	5.037	3.494
TOI1062	0.046	5328.0	4.55	0.13	0.1	2.347	0.000
BD-004475	0.072	5040.0	4.25	-0.14	0.1	2.959	0.056
alfAri	0.133	4513.0	2.49	-0.16	0.1	2.000	0.000
HIP109384	0.072	5185.0	4.39	-0.32	0.1	2.632	0.000
Kepler-418	0.135	5969.0	4.53	0.18	0.1	3.551	4.900
K2-10	0.047	5592.0	4.40	-0.01	0.1	2.927	0.192
HD109271	0.046	5794.0	4.27	0.11	0.1	3.590	0.000
HD28254	0.046	5664.0	4.12	0.06	0.1	3.612	0.000
HD42012	0.072	5353.0	4.38	-0.14	0.1	2.702	0.000

Table A.1. Parameters and results of the outliers.

Star	Instr broad	T_{eff}	logg	Fe/H	vsini	v_{mac}	e_{vsini}
38Vir	0.055	6440.0	4.42	0.16	28.767	5.674	2.288
CoRoT-11	0.055	6343.0	4.27	0.04	42.829	5.509	4.957
CoRoT-19	0.055	6317.0	4.38	0.17	6.679	5.171	0.845
CoRoT-1	0.061	6344.0	4.46	0.12	7.189	5.134	1.447
CoRoT-25	0.130	6104.0	4.30	0.16	4.610	4.466	0.902
CoRoT-2	0.055	5676.0	4.71	0.01	10.245	2.455	0.284
CoRoT-3	0.055	6558.0	4.25	0.14	17.46	5.500	1.174
CoRoT-4	0.110	6238.0	4.55	0.18	7.704	4.489	0.514
CoRoT-6	0.061	6265.0	4.60	0.01	9.789	4.503	0.900
DSTucA	0.130	5909.0	4.83	0.01	17.712	2.772	1.937
GJ3021	0.055	5563.0	4.48	0.06	4.198	2.723	0.780
HAT-P-34	0.130	6509.0	4.24	0.08	21.575	5.500	2.082
HAT-P-39	0.061	6721.0	4.79	0.22	14.328	5.500	1.919
HAT-P-45	0.061	6531.0	4.65	0.14	10.293	5.500	1.103
HAT-P-46	0.055	6344.0	4.43	0.36	4.658	5.194	0.432
HAT-P-50	0.061	6377.0	4.30	-0.05	8.445	5.608	0.700
HAT-P-66	0.135	6250.0	4.29	0.15	5.000	5.060	6.930
HATS-10	0.130	6167.0	4.51	0.40	5.757	4.283	1.419
HATS-27	0.055	6650.0	4.46	0.36	8.227	5.500	1.195
HATS-3	0.130	6347.0	4.52	-0.02	7.974	5.028	1.376
HATS-56	0.055	6594.0	3.98	0.25	5.525	5.500	0.791
HATS-58A	0.055	6564.0	4.35	0.13	4.596	5.500	0.820

HATS-66	0.061	7000.0	4.80	0.08	13.869	5.500	22.350
HATS-68	0.130	6276.0	4.43	0.24	7.331	4.891	1.792
HD103774A	0.055	6586.0	4.48	0.31	8.998	5.500	0.483
HD106315	0.061	6591.0	4.75	-0.06	13.993	5.500	1.513
HD10647	0.055	6178.0	4.49	-0.01	5.186	4.366	0.291
HD11231	0.055	6643.0	4.32	0.19	7.524	5.500	0.436
HD115954	0.072	5957.0	4.15	0.34	4.954	4.274	0.374
HD12484	0.072	5115.0	4.54	0.09	11.182	2.344	0.305
HD133131B	0.087	5751.0	4.37	-0.28	1.865	3.291	0.653
HD13908	0.097	6241.0	4.16	0.00	3.763	5.282	0.716
HD143105	0.072	6381.0	4.41	0.17	9.747	5.407	0.557
HD147873	0.055	6180.0	4.06	0.26	8.913	5.234	0.361
HD1666	0.055	6508.0	4.29	0.39	6.192	5.500	0.255
HD196885A	0.072	6312.0	4.43	0.25	7.327	5.049	0.467
HD19994A	0.055	6249.0	4.26	0.27	8.465	5.115	0.322
HD205739	0.055	6273.0	4.37	0.19	4.109	4.998	0.594
HD208487	0.055	6137.0	4.46	0.09	4.099	4.268	0.388
HD27969	0.072	5966.0	4.12	0.18	3.594	4.362	0.407
HD286123	0.055	5961.0	4.33	0.07	2.798	3.926	0.016
HD50499	0.055	6066.0	4.27	0.33	3.838	4.390	0.521
HD60532	0.055	6281.0	4.00	-0.07	6.628	5.772	0.591
HD63433	0.072	5671.0	4.49	0.00	7.077	2.885	0.201
HD66141	0.087	4357.0	1.99	-0.33	6.058	2.000	0.276
HD70573	0.130	5904.0	4.48	0.00	14.018	3.458	0.819
HD87646A	0.061	5949.0	4.28	0.28	8.725	3.990	0.257
HD93963A	0.072	5987.0	4.49	0.10	6.195	3.688	0.733
HR858	0.055	6360.0	4.50	-0.02	7.867	5.128	0.378
K2-100	0.055	6377.0	4.81	0.32	13.41	4.588	1.021
K2-290	0.055	6385.0	4.44	0.04	6.679	5.366	0.322
KELT-16	0.061	6514.0	4.45	0.09	6.488	5.500	0.746
KELT-4A	0.061	6478.0	4.34	0.00	6.680	6.026	0.463
KELT-6	0.055	6325.0	4.30	-0.23	4.210	5.367	0.809
Kepler-21	0.110	6323.0	4.21	0.05	6.685	5.538	1.004
Kepler-39	0.135	6556.0	4.78	0.06	13.155	5.500	8.326
Kepler-40	0.135	6296.0	4.48	0.01	8.570	4.878	1.753
Kepler-410A	0.110	6440.0	4.57	0.11	12.99	5.374	1.543
Kepler-435	0.135	6388.0	4.23	0.06	7.642	5.800	3.928
Kepler-539	0.135	5841.0	4.52	-0.02	8.862	3.207	0.502
Kepler-65	0.097	6374.0	4.41	0.23	8.717	5.374	0.642
Kepler-74	0.135	6956.0	4.41	0.34	4.999	5.500	0.961
Kepler-89	0.135	6306.0	4.44	0.10	7.907	5.002	0.891
Kepler-90	0.135	6142.0	4.47	0.15	5.472	4.267	1.165
KPS-1	0.135	4963.0	4.17	0.22	6.518	2.000	1.179
Pr0211	0.055	5250.0	4.37	0.16	5.281	2.678	0.135
TOI1298	0.072	5889.0	4.39	0.49	3.732	3.596	0.508
TOI-130	0.045	6203.0	4.50	-0.12	3.958	4.446	1.145
TOI-677	0.130	6300.0	4.52	0.14	6.929	4.816	1.012
TOI-813	0.055	6187.0	4.26	0.22	8.102	4.862	0.467
WASP-103	0.082	6188.0	4.48	0.29	10.759	4.425	1.149
WASP-113	0.135	6049.0	4.26	0.26	6.531	4.352	0.671
WASP-114	0.130	6110.0	4.44	0.51	5.899	4.208	1.098
WASP-118	0.061	6662.0	4.38	0.29	12.117	5.500	1.377
WASP-120	0.061	6774.0	4.62	0.15	16.424	5.500	2.916
WASP-135	0.135	5052.0	4.11	0.17	5.327	3.232	0.780
WASP-136	0.061	6770.0	4.57	0.18	14.867	5.500	1.064
WASP-138	0.061	6277.0	4.36	0.00	8.893	5.035	0.605
WASP-150	0.135	6486.0	4.46	0.27	8.778	5.827	0.670
WASP-153	0.135	5968.0	4.28	0.33	4.621	4.048	0.882
WASP-166	0.055	6142.0	4.45	0.25	4.869	4.307	0.364
WASP-173A	0.055	5803.0	4.45	0.21	6.978	3.252	0.309
WASP-174	0.055	6755.0	4.83	0.30	16.941	5.500	1.528
WASP-190	0.055	6730.0	4.52	0.15	14.153	5.500	0.827
WASP-20	0.055	6032.0	4.43	0.09	4.197	3.954	0.116
WASP-31	0.055	6380.0	4.59	-0.08	7.806	5.042	0.726

WASP-75	0.061	6102.0	4.37	0.24	5.597	4.319	0.317
WASP-84	0.055	5232.0	4.30	0.05	3.082	2.814	0.066
WASP-87A	0.061	6529.0	4.51	-0.28	11.190	5.500	1.804
WASP-90	0.061	6381.0	4.31	0.19	7.190	5.607	0.727
WASP-92	0.135	6039.0	4.21	0.10	6.533	4.418	1.272
XO-7	0.072	6109.0	4.30	0.40	5.933	4.484	0.495
TYC-3667-1280-1	0.047	5203.0	3.04	-0.04	3.732	5.332	0.455
HAT-P-20	0.046	4562.0	4.18	0.18	3.595	2.000	0.199
TOI-1130	0.046	4609.0	4.12	-0.07	3.081	2.000	0.273
NGTS-8	0.046	5781.0	4.37	0.1	4.074	3.359	0.600
BD+202457	0.047	4278.0	1.63	-0.74	4.423	2.000	0.108
HD27442	0.046	4801.0	3.39	0.31	3.081	2.000	0.193
CoRoT-9	0.046	5596.0	4.39	-0.02	0.666	2.954	2.300
HD159243	0.072	6077.0	4.44	0.01	4.532	4.089	0.388
HD141399	0.072	5571.0	4.10	0.30	3.267	3.495	0.410
K2-280	0.046	5763.0	4.30	0.34	8.795	3.458	0.103
WASP-76	0.046	6372.0	4.28	0.38	1.861	5.624	2.621
HD207832	0.047	5736.0	4.51	0.14	0.121	2.978	0.264
TOI1710	0.047	5665.0	4.46	0.10	3.539	2.934	0.622
HD238914	0.047	4876.0	2.59	-0.1	4.198	2.000	0.057
HATS-51	0.133	6043.0	4.78	0.49	2.499	3.291	2.747
CoRoT-22	0.135	5957.0	4.54	0.23	7.907	3.494	1.156
WASP-131	0.046	6138.0	4.22	-0.04	3.729	4.752	0.366
muLeo	0.109	4493.0	2.40	0.21	3.747	2.000	0.448
HD109286	0.072	5694.0	4.44	0.05	3.266	3.030	0.260
BD+152940	0.054	4797.0	2.63	-0.19	6.199	2.000	0.149
WASP-181	0.046	5943.0	4.44	0.20	4.423	3.652	0.342
K2-66	0.054	5956.0	4.10	-0.04	5.120	4.371	0.069
HD45184	0.047	5869.0	4.47	0.05	0.605	3.381	3.076
HD213885	0.046	5878.0	4.35	-0.01	2.854	3.646	0.427
HD16417	0.046	5848.0	4.14	0.14	0.240	3.986	0.342
Kepler-408	0.109	6142.0	4.33	-0.12	2.979	4.547	0.691
WASP-5	0.046	5764.0	4.36	0.22	3.723	3.340	0.286
WASP-91	0.054	5040.0	4.39	0.21	2.798	2.679	1.184
HIP63242	0.047	4832.0	2.54	-0.28	6.193	2.000	0.295
HAT-P-54	0.054	4540.0	4.13	-0.10	5.751	2.000	0.266
HATS-61	0.133	5845.0	4.50	0.50	3.253	3.258	2.616
HD133131A	0.046	5778.0	4.44	-0.25	0.286	3.212	0.288
WASP-52	0.054	5073.0	4.36	0.17	4.865	2.721	0.757
HR5183	0.072	5887.0	4.19	0.09	3.331	3.990	0.393
HD47186	0.047	5701.0	4.43	0.26	0.397	3.064	0.548
HD9174	0.046	5669.0	4.11	0.39	0.329	3.642	2.450
BD+152375	0.047	4701.0	2.34	-0.10	4.424	2.000	0.337
HD208897	0.047	4895.0	3.25	0.20	3.313	2.000	0.258
HAT-P-42	0.054	5870.0	4.22	0.35	4.897	3.884	0.657
HATS-17	0.047	5808.0	4.26	0.36	3.096	3.644	0.124
HAT-P-16	0.047	6250.0	4.49	0.21	3.601	4.66	0.359
betaCnc	0.054	4234.0	1.48	-0.29	6.290	2.000	0.427
K2-287	0.047	5633.0	4.29	0.26	0.424	3.216	0.396
omiUMa	0.109	5542.0	2.58	-0.16	1.825	6.493	0.182
Kepler-4	0.135	5885.0	4.17	0.19	3.986	4.025	0.614
K2-29	0.047	5327.0	4.36	0.16	4.199	2.727	0.128
HD124330	0.072	5873.0	4.24	0.22	2.332	3.852	1.972
HD92788	0.046	5762.0	4.31	0.29	0.214	3.436	0.429
HD221585	0.072	5638.0	4.05	0.29	0.621	3.705	2.324
HD208527	0.054	4118.0	1.83	0.08	8.365	2.000	0.391
HATS-14	0.133	5615.0	4.37	0.35	4.521	3.025	1.283
HATS-1	0.054	5930.0	4.46	-0.02	4.107	3.573	0.103
Kepler-1655	0.072	6112.0	4.45	-0.14	5.144	4.195	1.407
HD156411	0.047	5918.0	4.01	-0.10	2.798	4.438	0.362
91Aqr	0.046	4673.0	2.40	0.010	4.506	2.000	0.253
HD220842	0.072	5960.0	4.24	-0.17	3.098	4.103	0.485
HD5583	0.047	4900.0	2.65	-0.42	5.386	2.000	0.280
NGTS-10	0.133	4715.0	4.26	-0.09	4.606	2.000	0.460

WASP-145A	0.054	4748.0	4.22	-0.39	2.055	2.000	0.655
HATS-13	0.133	5485.0	4.51	0.14	2.789	2.56	2.671
HD9446	0.072	5775.0	4.46	0.03	4.018	3.165	0.487
K2-229	0.047	5125.0	4.34	-0.09	0.291	2.741	0.352
KOI3680	0.072	5830.0	4.47	0.16	5.416	3.279	0.808
WASP-156	0.046	4875.0	4.13	0.15	0.227	2.000	0.269
TYC4282-605-1	0.047	4558.0	2.61	0.07	3.732	2.000	0.163
omiCrB	0.109	4843.0	2.49	-0.21	3.172	2.000	1.888
WASP-124	0.133	6181.0	4.49	0.28	5.464	4.378	1.152
HATS-33	0.054	5718.0	4.37	0.33	4.622	3.219	0.530
HIP74890	0.054	4800.0	3.11	0.20	4.623	2.000	0.243
HD190984	0.046	6014.0	4.03	-0.46	3.096	4.695	0.604
K2-140	0.133	5955.0	4.58	0.50	3.264	3.408	1.537
muAra	0.047	5797.0	4.26	0.30	0.696	3.617	2.437
HD128311	0.072	4896.0	4.26	-0.03	3.957	2.000	0.244
piMen	0.046	6010.0	4.46	0.10	3.102	3.821	0.297
WASP-43	0.054	4652.0	4.32	-0.08	4.867	2.000	0.439
gamma1Leo	0.109	4447.0	1.99	-0.38	3.537	2.000	0.133
HD38677	0.046	6194.0	4.43	0.23	3.852	4.549	0.536
HD111591	0.054	4863.0	2.78	-0.13	4.872	2.000	0.456
HD331093	0.072	5544.0	4.20	0.17	0.223	3.256	0.420
HD150706	0.072	5942.0	4.53	-0.04	4.109	3.469	0.164
HD155193	0.072	6239.0	4.26	0.05	3.096	5.073	0.829
WASP-41	0.046	5508.0	4.40	0.04	3.081	2.808	0.137
epsTau	0.046	4921.0	2.75	0.19	5.197	2.000	0.240
Qatar-2	0.054	4505.0	4.01	0.14	4.430	2.000	0.920
epsCrB	0.054	4484.0	2.06	-0.10	6.665	2.000	0.150
TOI-1338	0.046	6095.0	4.36	0.00	5.309	4.313	0.304
K2-31	0.046	5413.0	4.37	0.16	3.096	2.767	0.040
K2-136	0.047	4494.0	4.33	0.01	2.608	2.000	3.190
14And	0.072	4745.0	2.52	-0.28	4.665	2.000	0.150
WASP-65	0.047	6245.0	4.29	-0.09	9.443	5.038	0.477
HD68402	0.047	5907.0	4.41	0.26	2.797	3.607	0.290
WASP-129	0.046	5982.0	4.38	0.18	3.883	3.892	0.439
WASP-122	0.054	5893.0	4.29	0.40	4.983	3.807	0.712
WASP-37	0.054	5811.0	4.30	-0.21	3.746	3.572	0.387
WASP-141	0.133	6217.0	4.52	0.53	5.812	4.462	1.272
HD35759	0.072	6018.0	4.15	-0.01	3.097	4.468	0.502
HIP65A	0.133	4712.0	4.30	0.05	3.595	2.000	0.571
HD17674	0.072	5909.0	4.36	-0.17	2.331	3.712	0.512
WASP-140	0.046	5307.0	4.39	0.01	4.198	2.657	0.223
HD134060	0.047	5965.0	4.45	0.14	2.798	3.699	0.168
WASP-64	0.133	5766.0	4.35	0.30	3.559	3.365	1.449
HD202206AB	0.047	5766.0	4.35	0.30	2.709	3.365	3.680

Table A.2. Parameters and results of all the stars with good values.